Suspended-sediment induced stratification inferred from concentration and velocity profile measurements in the lower Yellow River, China

Andrew J. Moodie[1], Jeffrey A. Nittrouer[1], Hongbo Ma[1], Brandee N. Carlson[1], Wang, Yuanjian[2], Michael P. Lamb[3]and Gary Parker[4,5]

[1]Department of Earth, Environmental and Planetary Sciences, Rice University, Houston, Texas, USA
[2]Yellow River Institute of Hydraulic Research, Zhengzhou, Henan 450000, China
[3]Division of Geological and Planetary Sciences, California Institute of Technology, Pasadena, California, USA
[4]Department of Civil and Environmental Engineering, University of Illinois at Urbana-Champaign, Champaign, Illinois, USA
[5]Department of Geology, University of Illinois at Urbana-Champaign, Champaign, Illinois, USA

Key Points:

- detailed concentration profiles reveal grain-size specific density stratification
- sediment diffusivity effects are overwhelmed by density stratification at high concentrations
- fine washload sediment ($< 25\ \mu$m) is vertically stratified in the Yellow River

Corresponding author: Andrew J. Moodie, amoodie@rice.edu

Abstract

Despite a multitude of models predicting sediment transport dynamics in an open-channel flow, the interaction between fluid and sediment, so to produce self-organized vertical density stratification, has not been robustly investigated and as such is poorly understood. This two-phase phenomenon develops in channels that possess low channel-bed slope and high sediment concentration. As the Yellow River, China, maintains one of the highest sediment loads in the world for a low sloping system, this location is ideal for documenting particle and fluid interactions that give rise to density stratification. Herein, we present analyses from a study conducted over a range of discharge conditions (e.g., low flow, rising limb, and flood peak) from a lower reach of the Yellow River, whereby isokinetic water samples were collected at targeted depths to measure sediment concentration and, simultaneously, velocity measurements were collected throughout the flow depth. Importantly, sediment concentration varied by an order of magnitude between base and flood flows. By comparing measured concentration and velocity profiles to predictive models, we show that the magnitude of density stratification increases with sediment concentration. Furthermore, a steady-state simulation of sediment suspension is used to determine that sediment diffusivity increases with grain size. Finally, we use this model to simulate concentration and velocity profiles over a spectrum of conditions that represent typical global river conditions during bankfull flow. We determine that the magnitude of density stratification can be predicted by a function that considers an entertainment parameter, sediment concentration, and bed slope.

1 Introduction

The interaction of sediment and water is a fundamental topic of sedimentology, and yet the development and effects of density stratification and the budget for turbulent kinetic energy in natural rivers are not well understood (e.g., M. H. García, 2008). Stratification develops where differences in fluid density arise due to, for example, temperature or salinity gradients (Turner, 1979). A stable stratification develops where a lower density fluid is positioned above a higher density fluid, and vertical mixing is inhibited. Suspended sediment in flows creates a stable stratification, because higher sediment-induced effective density is located near the bed (Turner, 1979). However, turbulent mixing disrupts density stratification, rendering it weak and often ephemeral in rivers (e.g., van Rijn, 1984). Measurements of stratification dynamics are limited, and so physical models are poorly constrained (Wright & Parker, 2004a). This research aims to assess predictions of flow velocity and sediment concentration dynamics, thereby advancing models for studies that seek to constrain sediment fluxes in lowland rivers and coastal deltas (Ma et al., 2020).

Sediment discharge in large, low-lying rivers is dominated by suspended transport (Milliman & Meade, 1983; Wright & Parker, 2004a, 2004b; Nittrouer et al., 2008). Suspended load is calculated by integrating the product of velocity and concentration over the cross-sectional area of flow:

$$q_s = \int^H \bar{u}(z)\bar{c}(z)\, dz, \tag{1}$$

where z is a quasi-vertical coordinate (i.e., assuming a low channel slope), H is the flow depth, $\bar{u}$ is the streamwise velocity (time-averaged), and $\bar{c}$ is the volumetric sediment concentration (time-averaged). Thus, accurate prediction of sediment transport in low-lying rivers and delivery to coastal deltas requires determining velocity and suspended sediment concentration depth-profiles.

Traditionally, models of velocity and concentration assume a dilute suspension, that is, a flow with small depth-averaged concentration (Rouse, 1937), whereby particles do not modulate flow. Experimental testing revealed that suspended sediment inhibits turbulent mixing due to density stratification, which increases the vertical velocity gradient, and changes the equilibrium sediment concentration profile (e.g., Vanoni, 1941, 1946; Einstein & Chien, 1955).

Stratified suspensions are known to exist in the field (e.g., Colby & Hembree, 1955; Nordin & Dempster, 1963), but have not been systematically explored, so as to determine the necessary conditions for the development of density stratification.

Herein, we present measurements of flow velocity and sediment concentration from the Yellow River, China, collected at river discharges varying over several orders of magnitude. We measured the grain-size distribution of each sample to determine grain-size specific effects of turbulent kinetic energy distribution, and used these measurements to improve theory for profiles of velocity and sediment concentration. In particular, we evaluate various models for concentration profiles in open-channel flow under stratified conditions, the behavior of sediment diffusivity with respect to fluid over flow depth and changes in sediment concentration, and modulation of sediment entrainment rates due to stratification. To our knowledge, this is the most detailed and comprehensive study of density stratification in a natural river system, to date.

2 Modeling the effects of density stratification

Open-channel flow structure is due to momentum redistribution through turbulent mixing (Turner, 1979). The Prandtl mixing length analogy is often utilized to close turbulent fluxes in one-dimensional profile modeling, which assumes an eddy viscosity profile (K_m) that varies parabolically with distance above the bed (Rouse, 1937; Doshi & Gill, 1970):

$$K_m = \alpha \kappa u_* z(1-(z/H)), \tag{2}$$

where $u_* = \sqrt{\tau_b/\rho}$ is the fluid shear velocity (a representation of basal shear stress τ_b in units of LT^{-1}, where ρ is fluid density), $\kappa = 0.41$ is the von Kármán constant (Einstein & Chien, 1955; Nezu & Rodi, 1986), and α is a depth-averaged adjustment to the eddy-viscosity profile which accounts for density-stratification effects due to sediment entrainment (Einstein & Chien, 1955; Wright & Parker, 2004b). A clear-water eddy viscosity profile (K_{m0}) is defined by the eddy viscosity adjustment coefficient $\alpha = 1$.

Integrating the eddy viscosity profile over z, and applying empirical closure for an integration constant $z_0 = k_s/30$ gives the log-law velocity profile for a steady, uniform, and hydraulically rough flow:

$$\frac{\bar{u}}{u_*} = \frac{1}{\alpha\kappa} \ln\left(30\frac{z}{k_s}\right), \tag{3}$$

where $k_s = 3D_{90}$ is the roughness height, and D_{90} is the 90^{th} percentile of the cumulative grain-size distribution of bed sediment (Nikuradse, 1926; van Rijn, 1984).

The vertical profile of sediment concentration for grain size i is (Rouse, 1937):

$$\frac{\bar{c}_i}{\bar{c}_{bi}} = \left[\frac{(H-z)/z}{(H-b)/b}\right]^{Z_{Ri}} \tag{4}$$

$$Z_{Ri} = \frac{w_{si}}{\alpha\kappa u_*}, \tag{5}$$

where $\bar{c}_{bi}$ is the time-averaged near-bed concentration for grain size i (at $z = b$, where b is a near bed elevation), and Z_{Ri} is the Rouse number for grain size i. The Rouse number characterizes the balance between particle settling velocity (w_{si}; computed herein via Dietrich, 1982) and the upward advection of sediment by turbulent eddies, which scales with shear velocity (u_*) (Figure 1b; Rouse, 1937; Vanoni, 1946). As $Z_R \to \infty$, sediment is concentrated near the bed, and as $Z_R \to 0$ sediment concentration is vertically uniform (Figure 1b).

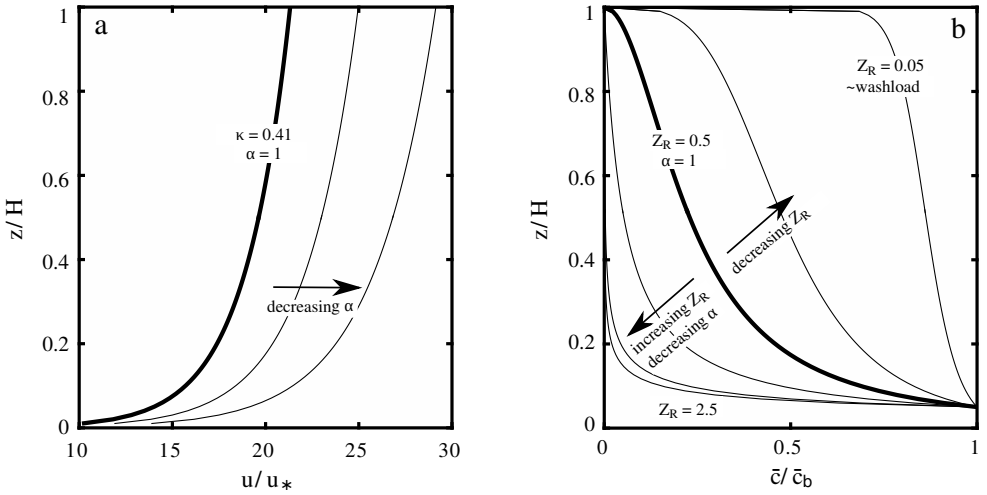

Figure 1: a) Dimensionless (normalized) log-law velocity profile calculated by Equation 3 for a shear velocity $u_* = 0.1$ m/s, flow depth $H = 3$ m, and roughness height $k_s = 4.8 \times 10^{-4}$ m. A decrease in α causes an increase in the velocity gradient. b) Dimensionless (normalized) Rouse profiles calculated by Equation 4. A decrease in α increases the Rouse number.

Numerous researchers have tested the velocity log-law and Rouse suspended sediment concentration profile relations with data collected from laboratory experiments (Vanoni, 1941; van Ingen, 1981; Coleman, 1986; Lyn, 1986; Nezu & Rodi, 1986; Villaret & Trowbridge, 1991; McLean et al., 1994; Ghoshal & Mazumder, 2005; Vanoni, 2006; Cornell, 2007), the field (Anderson, 1942; Barton & Lin, 1955; Colby & Hembree, 1955; Colby, 1964; Coleman, 1970; Smith, 1977; Smith & McLean, 1977a, 1977b; Vanoni, 1980; Coleman, 1981; van Rijn, 1984; Nittrouer et al., 2011), and through numerical simulations (Hsu et al., 2004; Amoudry, 2005; Chan-Braun et al., 2010). The log-law velocity and Rouse concentration relations are intended for dilute suspensions (Villaret & Trowbridge, 1991; Vanoni, 2006; M. H. García, 2008), and several assumptions, described in the following sections, are invalid for flows with high sediment concentration or a low channel-bed slope (van Rijn, 1984; Parker & Coleman, 1986; Wright & Parker, 2004a).

2.1 Density stratification

Suspended sediment increases the effective density of the fluid, and higher sediment concentration near the bed produces a vertical density gradient that induces a negative buoyancy and modulates eddy viscosity by increasing the dissipation of turbulent eddies. Hence, density stratification limits redistribution of momentum and sediment and invalidates the Prandtl mixing length assumption and parabolic eddy viscosity profile (Equation 2 Rouse, 1937; Wright & Parker, 2004a).

The gradient Richardson number characterizes the strength of density stratification (Smith & McLean, 1977b; Gelfenbaum & Smith, 1986; McLean, 1991, 1992; Wright & Parker, 2004b) by quantifying the balance of energy lost working against a density gradient to the turbulent kinetic energy generated by fluid shear:

$$\mathrm{Ri} = \frac{Rg\sum_{i=1}^{n} w_{si}\bar{c}_i}{u_*^2(1-(z/H))(d\bar{u}/dz)}, \tag{6}$$

where $R = (\rho_s - \rho)/\rho$ is the submerged specific gravity of sediment, ρ_s is the sediment density, g is the gravitational acceleration constant, and n is the total number of grain sizes in suspension (Turner, 1979; Wright & Parker, 2004b; Lamb & Parsons, 2005). A non-dimensionalized, depth-averaged, and cumulative grain-size (i.e., bulk) version of Equation 6 is given by the sand-river Richardson number (Wright & Parker, 2004a), where:

$$\mathrm{Ri}_{\mathrm{sr}} = R\frac{w_{s50}}{u_*}\frac{\bar{C}_m}{S_0}. \tag{7}$$

An alternative turbulence closure scheme that retains buoyancy effects demonstrates that density stratification is governed by the sediment dimensionless settling velocity (w_s/u_*), sediment concentration ($\bar{c}$), and water-surface slope (S_0) (i.e., Equation 7; Mellor & Yamada, 1982; Villaret & Trowbridge, 1991; Wright & Parker, 2004a). The sand-river Richardson governing parameters from several natural rivers show that the dimensionless settling velocity ($w_{s,50}/u_*$) varies independently of discharge and slope (Figure 2b). In contrast, the ratio of discharge-weighted sediment concentration to slope ($\bar{C}_m/S_0$, Figure 2a) increases significantly from low to high discharge in low-sloping rivers, but only mildly in steeper rivers. Further, Wright and Parker (2004a) identified a reduction in the depth-averaged eddy viscosity correlated with a decrease in $\bar{C}_m/S_0$ ratio (Figure 2c), and thus concluded that a low channel bed slope enhances density stratification effects (Wright & Parker, 2004a). However, for a given river, sediment concentration may vary by up to two orders of magnitude, whereas slope varies minimally over a wide range of discharges (Figure 2a). Thus, while the *potential* for density stratification is modulated by the channel-bed slope (Wright & Parker, 2004a), the actual magnitude of density stratification is principally dependent on sediment concentration. However, development of density stratification as a function of water discharge and sediment concentration in natural open-channel flows lacks complete understanding due to a lack of data.

A change in eddy viscosity over the flow depth is often parameterized as a function of the Richardson number (i.e., $K_m = K_{m0}\ f(\mathrm{Ri})$) (Smith & McLean, 1977b; Gelfenbaum & Smith, 1986; McLean, 1991, 1992; Wright & Parker, 2004b). Here, the eddy viscosity profile adjustment from Wright and Parker (2004b) is used: let $\overline{K}_{red} = \overline{K}_m/\overline{K}_{m0}$, the ratio of the depth-averaged sediment-laden fluid eddy viscosity ($\overline{K}_m$) to the depth-averaged clear-water eddy viscosity ($\overline{K}_{m0}$). Wright and Parker (2004b) cast the depth-averaged eddy viscosity reduction as the density-stratification adjustment coefficient α_{WP04} (Figure 2d):

$$\alpha_{\mathrm{WP04}} = \begin{cases} 1 - 0.06(\bar{c}_b/S_0)^{0.77} & \text{for } (\bar{c}_b/S_0) \leq 10 \\ 0.67 - 0.0025(\bar{c}_b/S_0) & \text{for } (\bar{c}_b/S_0) > 10 \end{cases}. \tag{8}$$

Decreasing α increases the vertical velocity gradient and lowers the suspended sediment concentration. The observations used to develop α_{WP04} (Equation 8) arise from applying a buoyancy-stratified model to solve for a sediment concentration profile using depth-averaged data, and then computing the depth-averaged eddy viscosity adjustment coefficient (Wright & Parker, 2004a, 2004b). However, the buoyancy-stratified model (Mellor & Yamada, 1982; Wright & Parker, 2004a) has not been rigorously tested against concentration or velocity profiles from natural river systems. A detailed description of this model is given by Yeh and Parker (2013).

We compare three models for velocity and concentration throughout the text: (i) Equations 3–5 for $\alpha = 1$ yield a dilute suspension prediction (denoted by variables with subscript 1.0), (ii) Equations 3–5 for $\alpha = f(w_s/u_*, \bar{C}, S_0)$ yield an α-stratified prediction (where a subscript on α denotes a specific prediction or analytical approach; Equation 8), and (iii) a buoyancy-stratified model that assumes Reynolds-averaged turbulent characteristics are in local equilibrium (the "Level 2-1/2" model; Mellor & Yamada, 1982; Galperin et al., 1988; Yeh & Parker, 2013) (denoted by variables with subscript MY).

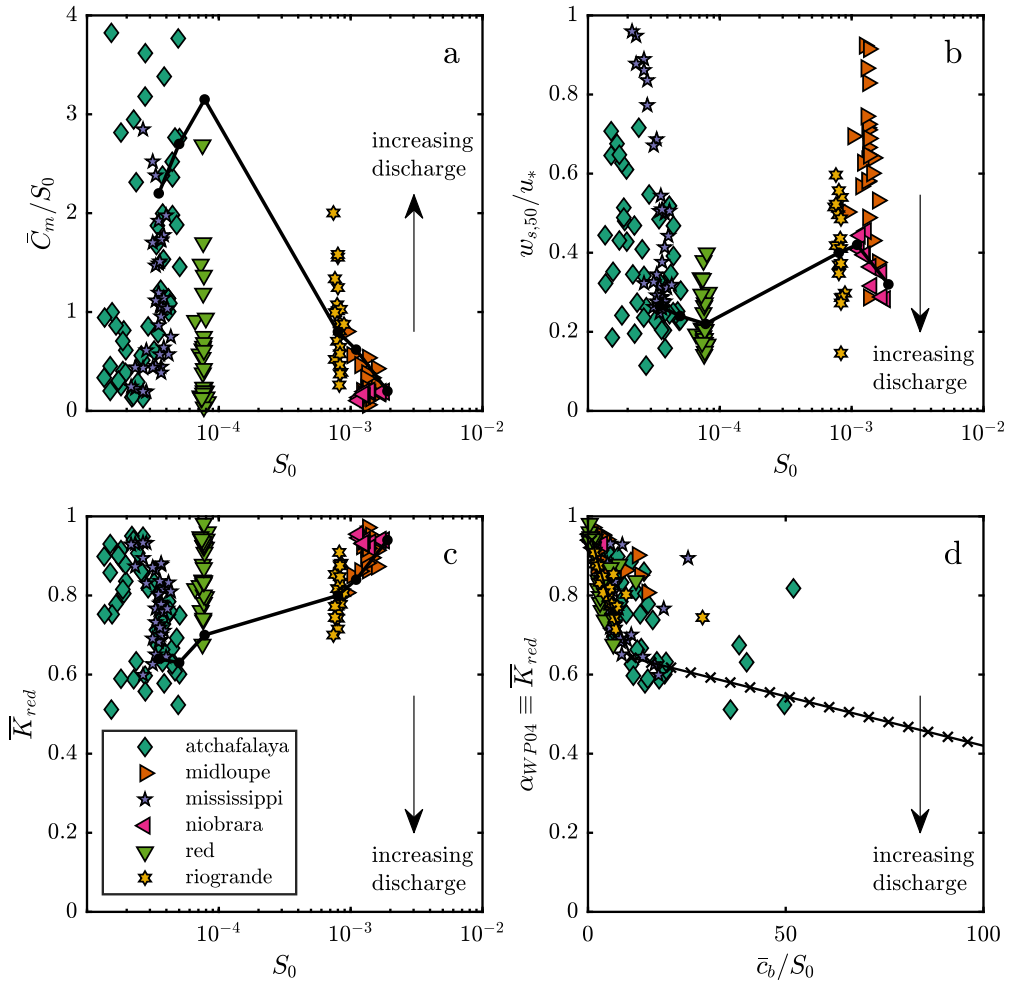

Figure 2: Selected figures after Wright and Parker (2004a, 2004b), displaying trends from six sand-bed rivers, and estimated values at 5% exceedance discharge. a) Ratio of total discharge-weighted suspended sediment concentration to slope versus slope. b) Dimensionless settling velocity versus slope. c) depth-averaged reduction in eddy viscosity versus slope. d) Predictive relationship for depth-averaged reduction in eddy viscosity (Equation 8).

2.2 Sediment diffusivity

The Rouse sediment concentration profile (Equation 4) and and buoyancy-stratified models assume that sediment diffusivity is equal to the kinematic eddy viscosity, whereby the sediment diffusivity coefficient $\beta = K_s/K_m = 1$ (Rouse, 1937; Rouse, Hunter, 1939). This definition implies that sediment diffusivity is not independent from density stratification, because each depends on eddy viscosity (K_m), which is modulated by stratification. Indeed, if the effects are assumed to interact linearly to modulate the Rouse number (i.e., if $Z_{R,i} = w_{s,i}/\beta\alpha_V\kappa u_*$), then the sediment diffusivity can be identified in the discrepancy between field measured concentration profile and velocity profile adjustments ($\beta = \alpha_f/\alpha_V$).

The behavior of sediment diffusivity β is frequently debated (Murray, 1970; Coleman, 1970; Jobson, 1970; Lees, 1981; van Rijn, 1984; Whitehouse, 1995; Cellino & Graf, 1999; Rose & Thorne, 2001; Graf & Cellino, 2002). Some suggest that higher sediment inertia (due to greater density) prevents an immediate response to turbulent velocity fluctuations ($\beta < 1$). Alternatively, higher sediment momentum could also thrust particles from eddies, and thus have a diffusive effect ($\beta > 1$). In actuality, the behavior of β likely varies with depth, and is dependent on both grain size and sediment concentration (Lees, 1981; Cellino & Graf, 1999; Greimann et al., 1999; Graf & Cellino, 2002; Amoudry, 2005; Ghoshal & Pal, 2014). The buoyancy-stratified model assumes a sediment diffusivity of $\beta = 1$, which enables a comparison between field data and modeled profiles to reveal the behavior of sediment diffusivity with respect to turbulence, as a function of grain size.

2.3 Sediment entrainment

The net vertical sediment flux near the bed depends on the balance of upward flux of sediment from the bed (the entrainment rate, E_r) as a function of transport stage, and a downward flux (the deposition rate, D_r) dependent on sediment concentration and settling velocity:

$$\bar{F}_{z=b} = E_r - D_r = w_s(E_s - \bar{c}_b), \tag{9}$$

where $E_s \equiv E_r/w_s$ is a dimensionless entrainment rate (i.e., volume per-unit-bed-area per unit time; M. H. García, 2008). At equilibrium, the net sediment flux ($\bar{F}_{z=b} = 0$) is zero, and the dimensionless entrainment rate is equivalent to the near-bed concentration, $E_s = \bar{c}_b$. As transport stage of the flow changes, entrainment and the near-bed concentration are modulated.

It remains unclear how turbulent dampening modulates sediment entrainment. Intuitively, it may be expected that the sediment entrainment rate is reduced by dampening of turbulence intensity and magnitude of entraining turbulent eddies; however, a near-bed sediment-laden fluid layer could minimize drag from the channel bed, and thus sustain a shear velocity consistent with an unstratified flow (Vanoni, 1941). Turbulent kinetic energy is consumed by the near-bed density gradient over a shortened length (height) scale, and energy is utilized to keep sediment in suspension (e.g., M. García & Parker, 1991, 1993). The relationship between density stratification and entrainment has not been explored experimentally or with data from natural open-channel flows.

Many entrainment relations exist in the literature, with a wide range of necessary parameters (reviewed in M. H. García, 2008). The relations are typically of the form: $E_s = f(\tau_b, D, \ldots)$, where parameters other than τ_b and D include critical stress of mobility (τ_{cr}), slope (S), and/or Richardson number (Ri) (van Rijn, 1984; M. H. García, 2008). Wright and Parker (2004b) develop a relation that depends on the channel bed slope and thus incorporates the

effects of density stratification:

$$E_{si} = \frac{B(\lambda X_i)^5}{1 + \frac{B}{0.3}(\lambda X_i)^5} \tag{10}$$

$$X_i = \left(\frac{u_{*,sk}}{w_{si}}\mathrm{Re}_{\mathrm{p}i}^{0.6}\right) S_0^{0.08} \left(\frac{D_i}{D_{50}}\right)^{0.2}, \tag{11}$$

where X_i is the entrainment parameter of grain class i, $\lambda = 1 - 0.28\sigma_\phi$ where σ_ϕ is the standard deviation of the channel-bed sediment in the sedimentological ϕ scale, $B = 7.8 \times 10^{-7}$ is an empirical constant, $u_{*,sk} = \sqrt{\tau_{*,sk} R g D_{50}}$ is the component of shear velocity partitioned as skin friction on the bed and $\tau_{*,sk} = 0.05 + 0.7(\tau_* \mathrm{Fr}^{0.7})^{0.8}$ where $\mathrm{Fr} = U/\sqrt{gH}$, $\mathrm{Re}_{\mathrm{p}i} = (\sqrt{RgD_i}D_i) \ / \ \nu$ is the particle Reynolds number of grain class i, where ν is the kinematic viscosity of the fluid, D_i is the characteristic diameter of grain-class i, and D_{50} is the median grain diameter of the bed sediment (M. García & Parker, 1991, 1993). A potential problem with this approach is that density stratification effects are fixed for a given slope (in contrast to Figure 2b; Wright & Parker, 2004a). This model provides some consideration of density stratification effects through the Froude number and shear stress partitioning; however, it is not clear whether this will capture the full range of density stratification in a river.

3 Yellow River fluvial system

Density stratification is expected to develop in low-slope and high sediment concentration flows (Wright & Parker, 2004a). The Yellow River is thus an ideal natural laboratory to explore the development and effects of density stratification on hydrodynamics and sediment transport. The Yellow River flows across northern China, generally from west to east, draining an area of 752,000 km^2 over a river length of 5,460 km, before entering the Bohai Sea (Figure 3) (van Gelder et al., 1994; Ren & Walker, 1998; Saito et al., 2000). The drainage basin includes the Loess Plateau, an unconsolidated sediment deposit ∼100 m thick comprised of very-fine sand and silt (Saito et al., 2001; Yu, 2002; Ma et al., 2017), which is readily eroded and contributes to the large sediment discharge of the Yellow River (1 Gt/yr Yu, 2002). With a bankfull discharge of 3,000–4,000 m^3/s, sediment concentration in the lower Yellow River is remarkably high, approximately one to two orders of magnitude greater than other large lowland rivers (e.g., Mississippi River and Amazon River) (Wang & Liang, 2000; Yu, 2002). In the lower Yellow River (lowermost ∼200 km) bankfull flow depth ranges 2–6 m, and channel width averages 400 m. Channel bed slope in the lower Yellow River takes the approximately constant value 6.4×10^{-5} (Moodie et al., 2019). Yellow River sediment concentration varies by several orders of magnitude as a function of water discharge (Ma et al., 2017; Moodie et al., 2019), which provides the opportunity to study development of density stratification with progressively changing sediment concentration.

3.1 Field measurements

Three field campaigns in the summers of 2015, 2016, and 2018 were conducted between 80–100 km upstream of the river mouth, near the cities of Kenli and Lijin (Figures 3, 4a; Moodie, 2019). This reach of channel is upstream of backwater influence (Ganti et al., 2014; Moodie et al., 2019). Field survey objectives included collecting water column velocity and concentration measurements over a range of water discharge conditions from 21 stations (Figure 4).

During the 2015 survey, a single point-integrated water sample (1 liter) was collected at three fixed heights above the bed ($z/H = 0.05$, 0.25, and 0.5), and a channel bed grab sediment sample was collected to assess bed material

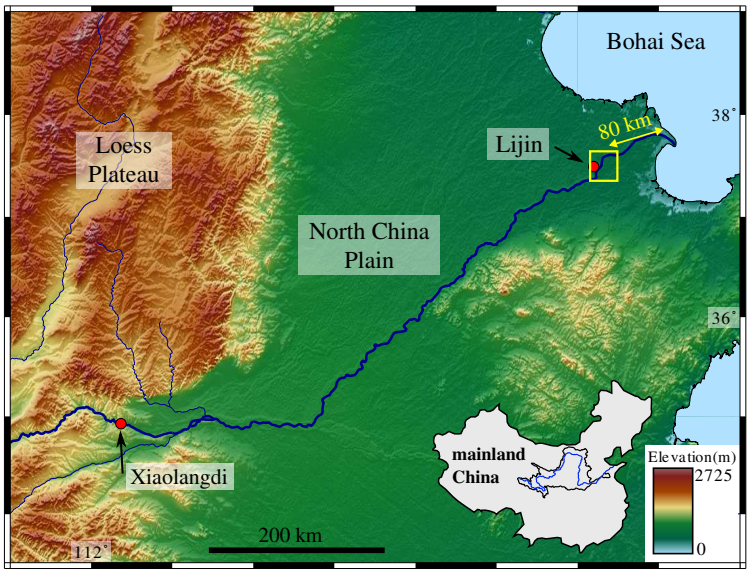

Figure 3: Map of the lower Yellow River; inset shows drainage basin and course of Yellow River across mainland of China. The study area is 80–100 km upstream of the river mouth, the yellow box contains the map areas shown in Figure 4.

grain size (Figure 5a). In the 2016 and 2018 surveys, a bed sediment sample and three water and suspended sediment samples were collected at five points above the bed ($z/H = 0.05$, 0.15, 0.25, 0.5, and 0.9) for a total of 15 samples at each station (Figure 5b–c). Suspended sediment samples were collected using a temporal window of 15–30 seconds. Three samples collected at each height provided a means to accurately constrain the mean sediment concentration and grain-size distribution in the flow (Gitto et al., 2017).

Water samples were processed to determine sediment concentration by measuring total sample water volume, weighing the dried samples, and assuming a sediment density of 2650 kg/m^3. The grain-size distribution of each sample (suspended sediment and channel bed samples) was determined by laser diffraction in a Malvern Mastersizer 2000 instrument. The washload fraction of the suspended sediment samples was removed by excluding the fraction of sediment less than 15 μm (Figure 5a–c; Ma et al., 2017), and the grain-size distributions were renormalized and cast into a logarithmically-spaced six-class distribution. Stations where the cumulative concentration profile did not monotonically increase with depth were identified as outliers (n=7), and plotted as open symbols in figures herein.

Sample processing resulted in more than 1,700 grain-size specific sediment concentration measurements that span the range of flow depth and discharge of the lower Yellow River. In order to evaluate the data on a per-station basis, grain-size specific profile statistics are combined by a weighted average (based on the probability density function of the grain-size distribution) to yield a single bulk statistic characterizing the station.

3.2 Survey measurements

The samples in this study are all collected from the same reach; water surface slope, $S_0 = 6.4 \times 10^{-5}$, is measured from a shipboard navigation system (Moodie et al., 2019). Measured sediment concentration from all surveys are shown in Figure 5d–f. Floods during the 2015 and 2018 field surveys (>2,000 m^3/s) generated near-bed sediment

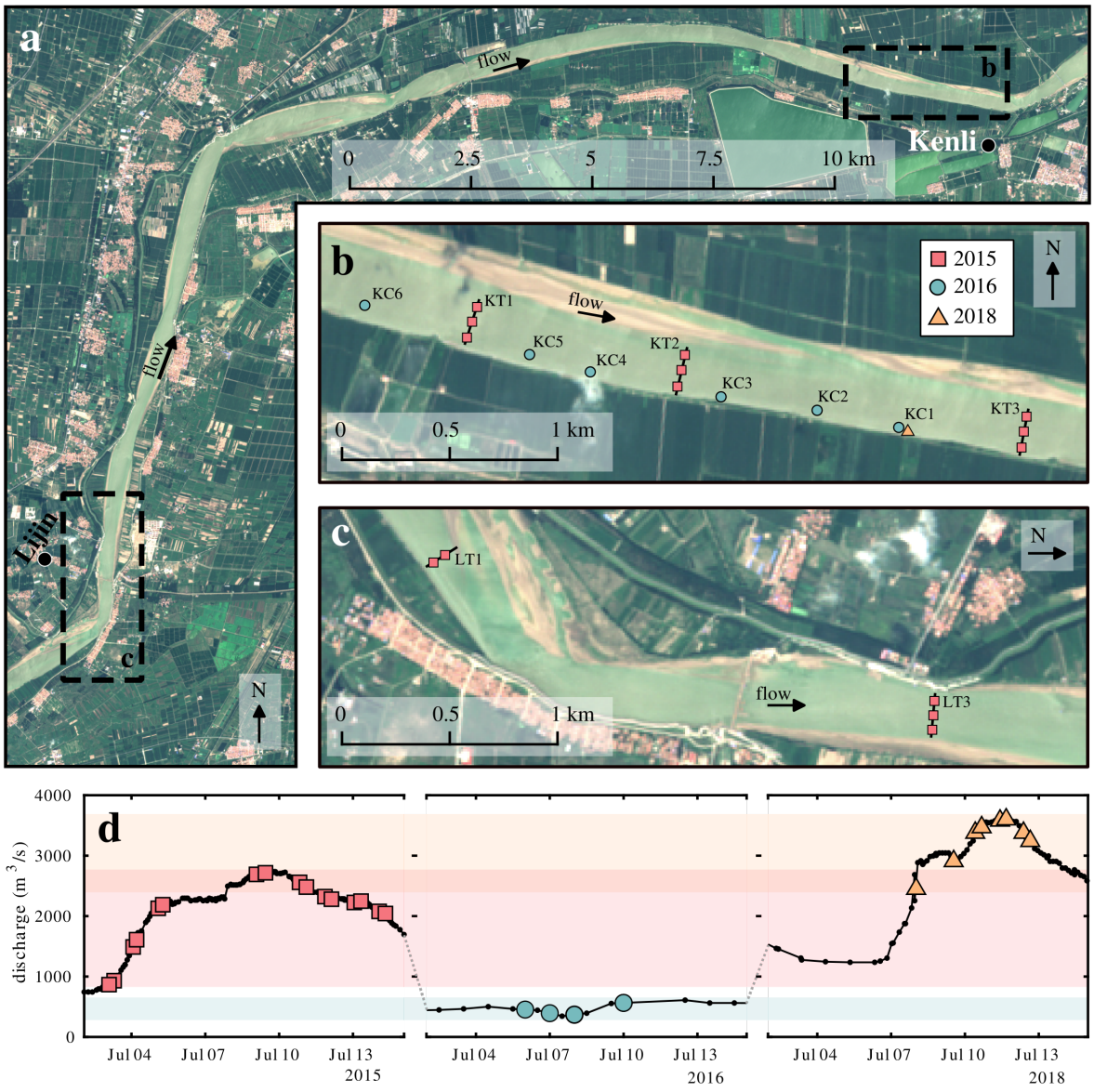

Figure 4: a) Overview of survey reaches from this study, Lijin (upstream) and Kenli (downstream), located ∼24 km from one another. b) Field survey map of the Kenli survey reach. KT- refers to a transect along which three stations are located (2015 survey). KC- refers to a station from 2016 or 2018. c) Field survey map of the Lijin survey reach. LT- refers to a transect along which 2–3 stations are located (2015). Images from Sentinel 2 satellite, February 10 2016. d) Composite hydrograph from three survey years; symbols denote timing of station surveys, which cover the full range of the hydrograph.

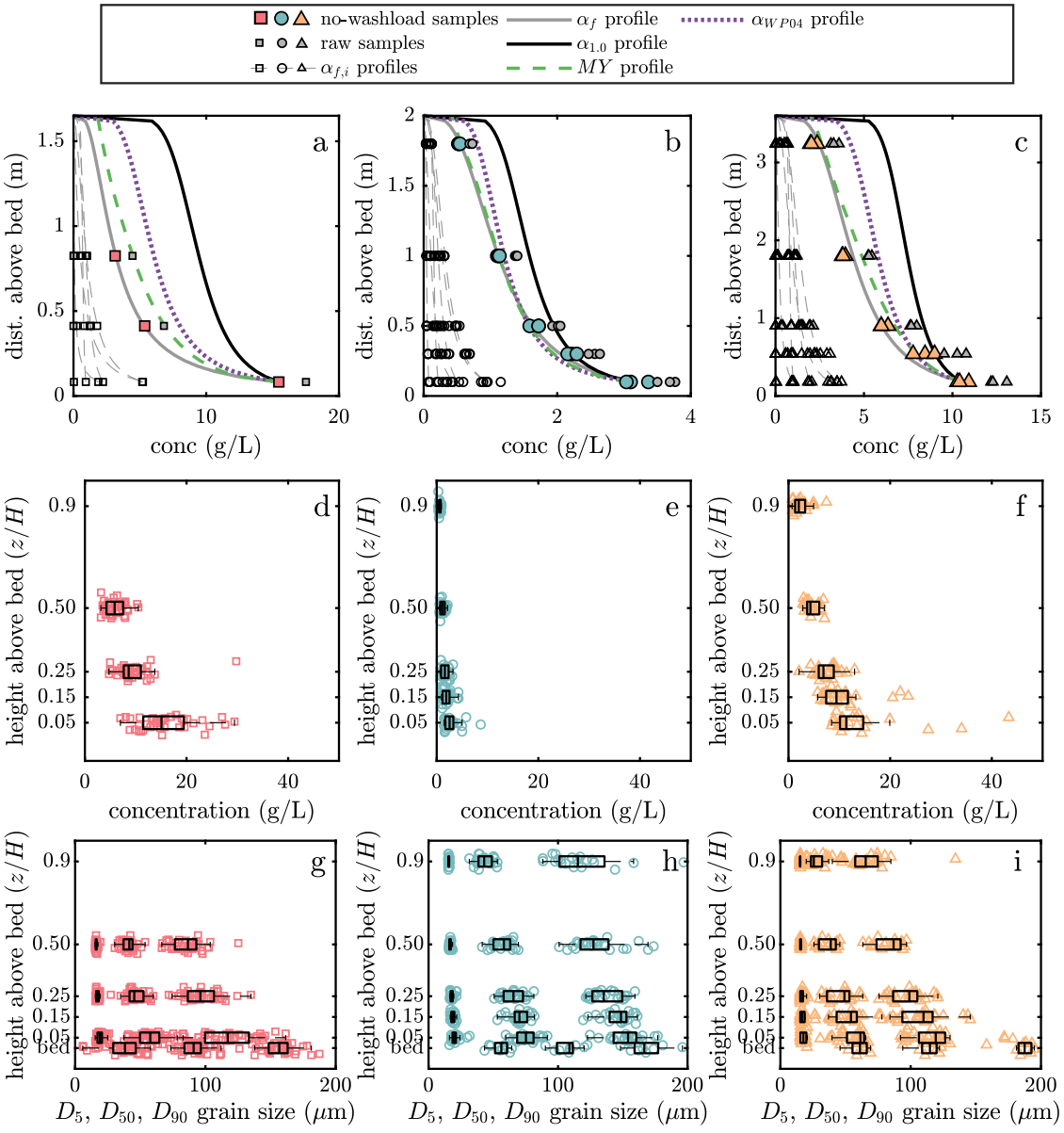

Figure 5: a–c) Representative 2015, 2016, and 2018 stations with sediment concentration measurements and modeled profiles. Blue horizontal dotted line is the water surface, measured water-sediment samples are open symbols, filled symbols are after removing the washload fraction, thick gray line is the summed profile of grain-size specific best-fit concentration profile models (thin gray lines), black solid line is prediction based on α-stratified concentration profile model without density stratification effects (Equation 4–5, $\alpha = 1$), and black dashed line is buoyancy-stratified model evaluated for the station. d–f) Boxplots of sediment concentration as a function of normalized collection height, for each survey year. g–i) Boxplots of D_5, D_{50}, and D_{90} for all suspended sediment and channel-bed samples, for each survey year.

concentration in excess of 30 g/L. In contrast, without a flood, the near-bed concentration during the 2016 survey is, on average, 80% lower than 2015 and 2018. Overall, the measured concentration decreases with increasing distance above the bed (Figure 5d–f). Multiple samples collected from the same depth show little variability in concentration or grain-size distribution (Figure 5), which provides evidence that the concentration profiles reflect time-averaged values. Velocity profiles were fit with a log-law model (Equation 3) to determine local shear velocity (Nittrouer et al., 2012, Supplementary Material).

The median grain size of the bed sediment is 90–120 μm across all survey years (Figure 5g–i). Bed material samples from 2015 are finer than 2016 and 2018. This may be the result of a different collection technique that introduced very-fine suspended sediment into the sample. Overall, the grain-size distributions of measured suspended sediment fine with increasing distance from the bed. Additionally, the percentage of washload measured in the suspended sediment samples increases with distance above the bed, from 20–30% near the bed, to 50–60% near the surface (Supplementary Material). At the Kenli reach, the Yellow River channel bed is remarkably flat: long-wavelength bedforms do little to disrupt or extract momentum from the flow (Ma et al., 2017).

3.3 Shear velocity calibration

In 2016 and 2018, water velocity profile measurements were made at each station with an acoustic Doppler current profiler (aDcp) and a mechanical propeller-driven velocimeter. Local shear velocity was determined by a best-fit regression to the measured velocity profiles, and combined with water discharge data (collected $\sim$10 km upstream at a nearby gauging station operated by the Yellow River Hydrological Bureau), to produce a reach-scale relationship for shear-velocity (Figure 6):

$$u_{*,\mathrm{calib}} = -0.064[\log_{10} Q_w]^{0.009}[H]^{0.042}. \tag{12}$$

This method of fitting is sensitive to measurements made by the mechanical velocimeter near the bed, and could lead to overestimates of the shear velocity. The effects of form drag on shear stress partitioning (Wright & Parker, 2004a), including bedforms (McLean, 1991, 1992; McLean et al., 1994), are ignored in computing shear velocity, except where the stress is reduced to the skin-friction stress value (denoted by the subscript *sk*), for exploring entrainment rates.

Velocity profile data were not collected in the 2015 survey, and so a relationship for flow depth and shear velocity was initially substituted (i.e., depth slope product, $u_* = \sqrt{gHS_0}$; Leopold et al., 1995). However, the only varying parameter in the DSP calculations is the flow depth (H), and local variability in flow depth is poorly correlated to reach-averaged shear stress and suspended sediment concentration (e.g., An et al., 2018, Figure 6).

4 Measuring effects of density stratification

4.1 Density stratification

Density stratification was identified by comparing measured concentration profiles ($\bar{c}_f$) to predictions from a dilute-suspension model ($\bar{c}_{1.0}$). The measured sediment concentration profiles of each grain-size class ($c_{f,i}$) were fit with Equation 4, where $\bar{c}_{b,i}$ and $Z_{Rf,i}$ are free parameters. The grain-size specific models were cumulated to produce a best-fit concentration profile for the station ($\bar{c}_f$), where the bulk Rouse number (Z_{Rf}) is a weighted average of the grain-size class Rouse numbers (Figure 5a–c). The measured near-bed grain-size distribution and concentration data were

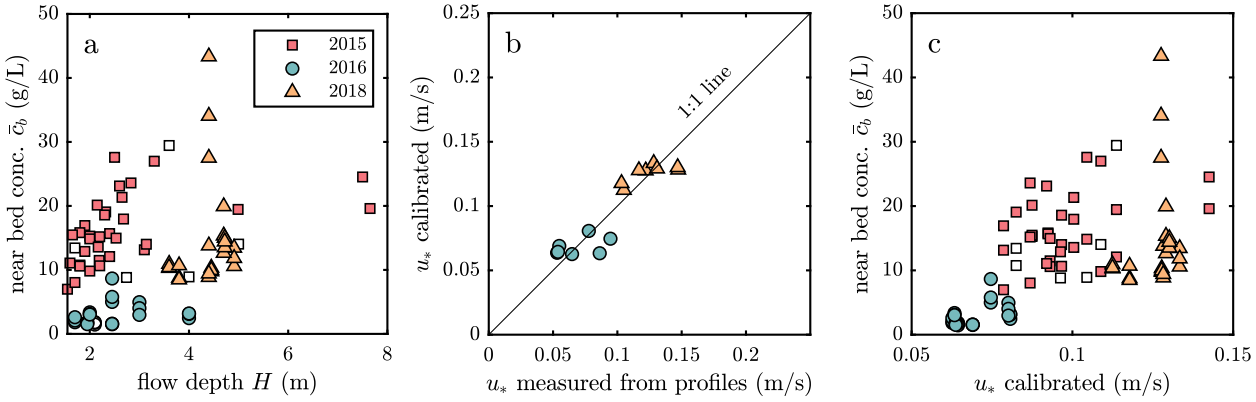

Figure 6: Calibration for u_* for all measurements. a) near bed concentration is poorly correlated with the local flow depth. b) a calibration (Equation 12) using u_* derived from velocity profiles in 2016 and 2018, and discharge measured at Lijin station. The calibration smooths local variations in depth and shear velocity that may not be reflected in corresponding suspensions, and c) improves correlation between shear velocity and near bed concentration.

used to evaluate grain-size specific concentration profiles according to the (i) dilute-suspension ($\bar{c}_{1.0,i}$), (ii) α_{WP04}-stratified ($\bar{c}_{WP04,i}$), and (iii) buoyancy-stratified ($\bar{c}_{MY,i}$) models. These grain-size specific predictions were cumulated according to the same procedure as the fit profiles to produce bulk statistics.

The normalized mean signed deviation for grain size class i ($\hat{\theta}/\bar{c}_{b,i}$) between a dilute-suspension ($\bar{c}_{1.0,i}$) and best-fit ($\bar{c}_{f,i}$) model pair was calculated as:

$$\frac{\hat{\theta}_i}{\bar{c}_{b,i}} = \frac{\sum_{\hat{z}=1}^{p}[\bar{c}_{1.0,i}(\hat{z}) - \bar{c}_{f,i}(\hat{z})]/p}{\bar{c}_{b,i}}, \tag{13}$$

where $\hat{z}$ is a discrete mapping of vertical coordinate z, and $p = 51$ is the number of points where the models are evaluated. Similarly, the mean signed deviation was calculated between a cumulated dilute-suspension ($\bar{c}_{1.0}$) and best-fit ($\bar{c}_f$) model pair. This statistic characterizes the degree of error for the dilute-suspension model, where $\hat{\theta}/\bar{c}_b > 0$ implies a density stratification effect (Figure 7a).

The error between the cumulated dilute-suspension model is approximately zero for low values of the dimensionless shear velocity, but a mis-prediction persists for stations with larger dimensionless shear velocity values, which correlate to higher sediment concentrations (Figure 7a). There is a positive relationship between dimensionless shear velocity and normalized mean signed deviation for each grain-size class (note the symbol sequence, circle→square→triangle, for each grain-size class, Figure 7b). However, the grain-size specific normalized mean signed deviation scales predominantly with dimensionless shear velocity due to the different grain-size classes, rather than variable flow conditions. Specifically, $\hat{\theta}_i/\bar{c}_{b,i}$ increases with dimensionless shear velocity, from approximately zero for the coarsest grain-size class, but decreases in the smallest two grain-size classes (Figure 7b).

The adjustment coefficient in the Rouse number (Equation 5) necessary to produce a measured sediment concentration profile is given by $\alpha_{f,i} = Z_{Rf,i}/Z_{R1.0,i}$ for each grain-size class i, because α is assumed to be unity in the dilute-suspension model $\bar{c}_{1.0,i}$. The grain-size specific concentration profile $\alpha_{f,i}$ values were cumulated to a bulk α_f statistic for each station, which was compared to the regression for α (Equation 8, Figure 8a; Wright & Parker, 2004b).

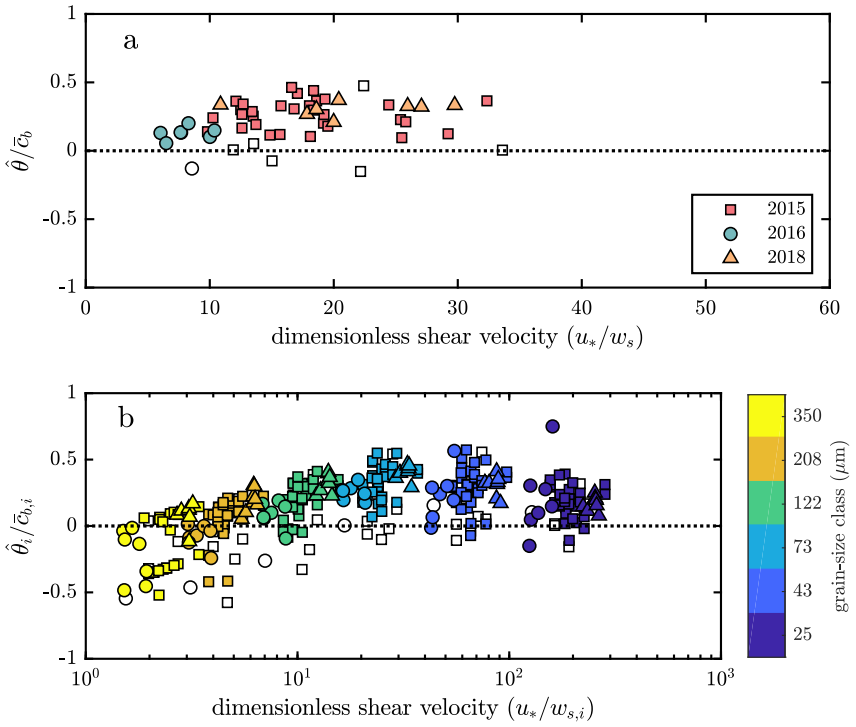

Figure 7: a) Normalized mean signed deviation of $\bar{c}_{1.0}$ and $\bar{c}_f$ (Equation 13) as a function of dimensionless shear velocity. Differences in the profiles are apparent only in samples collected under larger dimensionless shear velocity conditions. b) Grain-size specific normalized mean signed deviation (Equation 13). Misprediction of the dilute-suspension models scales primarily with the grain-size class.

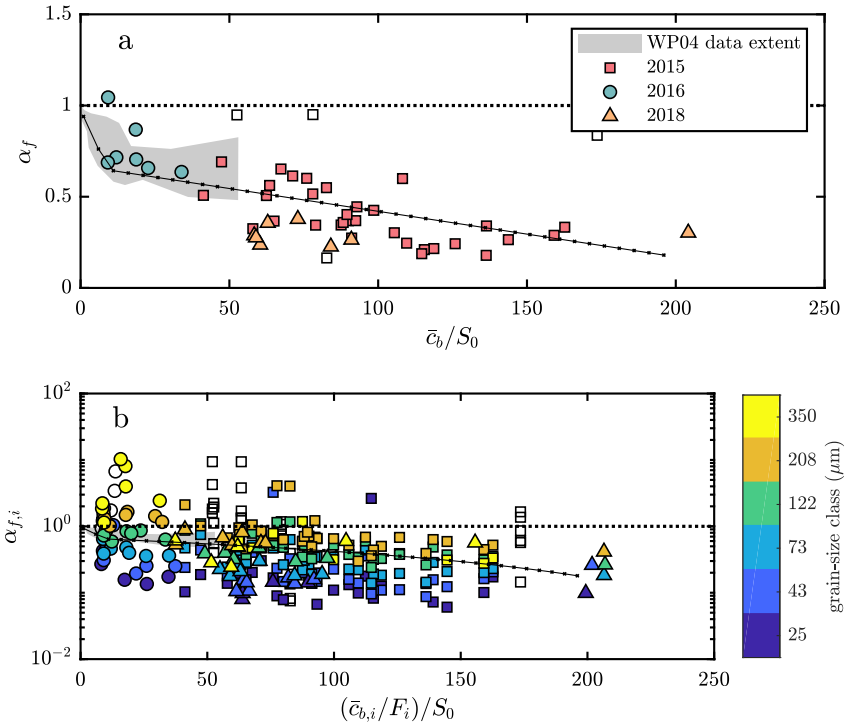

Figure 8: a) α_f calculated by the ratio of the field measured Rouse number to Rouse number from the dilute-suspension model. b) Grain-size specific $\alpha_{f,i}$.

A larger density stratification effect (decreasing α) occurs with increasing near-bed concentration-to-slope ratios (Figure 8a). The Yellow River data provide much higher $\bar{c}_b/S_0$ ratios than previously measured in the field, and coincide with the α_{WP04} prediction (Equation 8; Wright & Parker, 2004b). The grain-size specific calculations show a similar trend, but the $\alpha_{f,i}$ coefficient for different grain-size classes decreases as the grain size decreases (Figure 8b): smaller grains are more stratified for the same $\bar{c}_b/S_0$ ratio. The grain-size specific stratification calculation is sensitive to poorly-fitting concentration profiles of the coarsest and finest grain-size classes. For example, a very low concentration of sediment > 208 μm yielded $\alpha_{f,i}$ values that are > 10 (Figure 8b). Similarly, the finest grain-size class yielded spurious $\alpha_{f,i}$ values due to the minute concentration of fine sediment in suspension (recall that washload < 15 μm was removed from the calculations).

The α_{WP04} model consistently over-predicts the cumulative concentration profile, especially so in the upper portions of the water column (Figure 5, Supplementary Material). This is the result of applying a single α value to each individual grain-size profile prediction: the concentration profiles are mismatched to the measured profiles in the coarsest and finest grain-size classes. However, the concentration of sediment in the coarse grain-size class is relatively small, and so the over-prediction results from applying too large an α value for the finer grain-size classes.

Larger sand-river Richardson numbers correspond to increasing density stratification (Figure 9a). Interestingly, the trend of the Wright and Parker (2004a) model for sand-bed rivers is extended by adding the Yellow River data. The shape of the concentration profile was characterized by the recovery coefficient

$$r_0 = \bar{c}_b/\bar{C}_m, \tag{14}$$

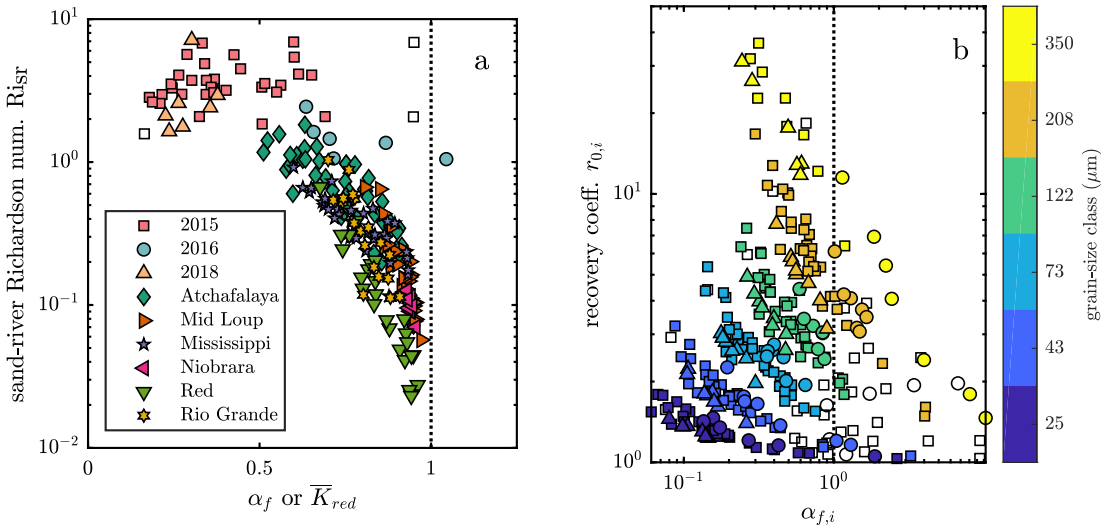

Figure 9: a) Sand-river Richardson number (Equation 7) and b) recovery coefficient (Equation 14) as a function of the depth-averaged reduction in eddy viscosity.

where a value ≥ 1 is expected for open-channel flows, but this value varies considerably as a function of environmental parameters (Zhang et al., 2013; Duan & Nanda, 2006; Cao et al., 2006; Zhang & Duan, 2011). Each grain-size class shows an increase in the recovery coefficient with increasing stratification effects (decreasing $\alpha_{f,i}$). The r_0 values for the finest grain-size class are ≥ 1 (i.e., stratified) for all measured conditions. r_0 values for coarser grains-size classes (≥ 122 μm) increase approximately exponentially as a function of the density stratification increase, reaching an r_0 value of $\sim$12 for the coarsest grain-size classes. The exponential trend for each grain-size class trend has a different intercept (i.e., a different r_0 for $\alpha_{f,i} = 1$).

4.2 Sediment diffusivity

The measured concentration profiles are also modulated by the sediment diffusivity coefficient (β), which describes the relationship between sediment and water transport in turbulent eddies. Thus, the metrics above incorporate both sediment density stratification and sediment diffusivity; herein the impact of sediment diffusivity is examined. The sediment diffusivity coefficient was elucidated by comparing the α_f value derived from the sediment concentration profiles with an adjustment coefficient derived from the measured velocity profiles at the same station (α_V). Note that this is a functionally equivalent approach to the "apparent von Kármán number" κ_a from Einstein and Chien (1955), where $\kappa_a = \kappa\alpha_V$ (Wright & Parker, 2004b). α_V was determined by the slope of a best-fit line to the velocity profile measurements in log-linear space while holding the shear velocity fixed (Figure 10a, Supplementary Material).

The stratification coefficients derived from the velocity and concentration profiles were approximately equal and near unity for the 2016 data, which show minimal density stratification ($\alpha_V \approx \alpha_f$, Figure 10a). Both profile adjustments are less than unity for 2018, when there was considerable density stratification. Interestingly, the adjustment to the concentration profile exceeds the adjustment to the velocity profile (Figure 10a).

The sediment diffusivity coefficient can be directly recovered from the density stratification adjustment coefficient α_V, if the effects are assumed to interact linearly to modulate the Rouse number (i.e., if $Z_{R,i} = w_{s,i}/\beta\alpha_V\kappa u_*$).

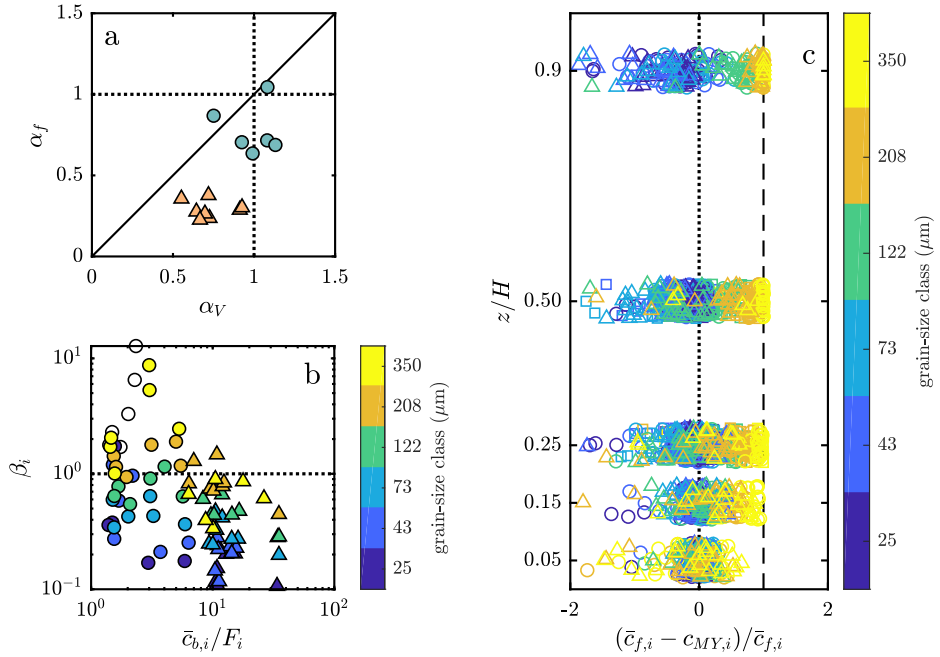

Figure 10: a) Comparison plot of α_V determined from the fit to velocity profiles versus α_f fit to the concentration profiles. b) β as a function of concentration. c) Ratio of measured sediment concentration over the concentration predicted by the buoyancy-stratified model.

Under this assumption, $\beta = \alpha_f/\alpha_V$. The sediment diffusivity coefficient of each grain-size class decreases with increasing near-bed concentration (Figure 10b).

The buoyancy-stratified model assumes that the sediment diffusivity coefficient is equal to unity ($\beta = 1$); the ms-match between the measured and buoyancy-stratified concentrations thus informs the *actual* sediment diffusivity in the flow. The fractional error with respect to the measured samples is calculated for each grain-size class $((\bar{c}_{f,i} - c_{MY,i})/\bar{c}_{f,i})$ and examined as a function of distance above the bed (Figure 10c). A fractional-error value of zero indicates that the buoyancy-stratified model matches the measurement, a fractional-error value < 0 implies sediment inertia leads to diffusivity less than the fluid eddy diffusivity ($\beta < 1$), and a fractional-error value > 0 implies momentum carries sediment beyond fluid eddies ($\beta > 1$).

There is an overall increase in the variability of the fractional error metric (positive and negative) with increasing distance above the bed (Figure 10c). Additionally, the finer grain-sizes tend slightly towards negative fractional error values, whereas the coarser grain-size classes tend towards the upper limit value of 1 (Figure 10c). Note that the buoyancy-stratified model uses the field-measured near-bed concentration and grain-size distribution as boundary conditions. The prediction thus matches the data measured near the channel bed due to proximity to the boundary.The precise fractional error value should be interpreted with caution, because the metric has an upper bound at unity, and is sensitive to low concentration predictions from the buoyancy-stratified model.

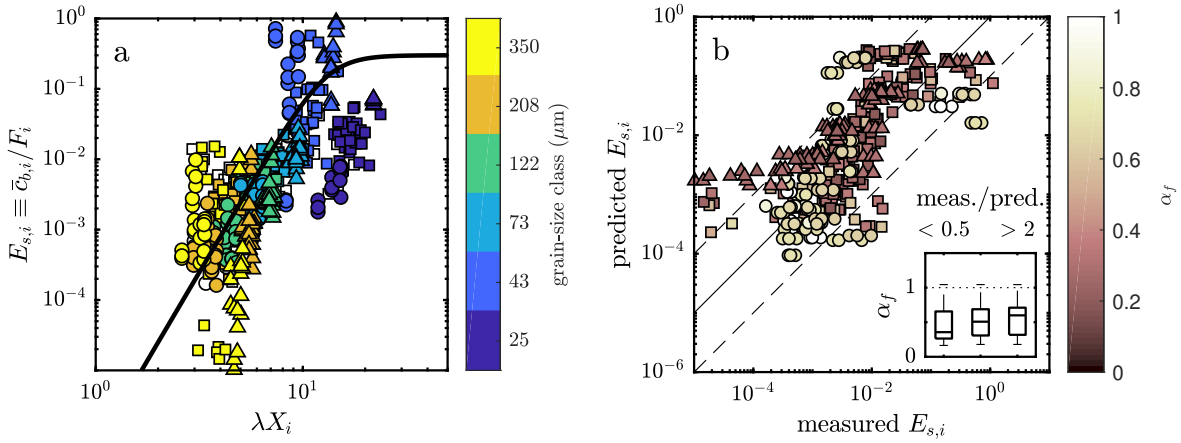

Figure 11: a) Near-bed concentration as a function of the grain size sorting (λ) and entrainment parameter X_i. Black line is the prediction by Equation 11 (Wright & Parker, 2004b). b) Correlation between measured and predicted concentration (using Equation 11); outliers are omitted. Dashed lines represent one order of magnitude from the 1:1 line. Inset) boxplot of stratification effect α_f for $E_{s,i}$ measurements, grouped by the factor by which the measured exceeds the predicted (axis label above inset). Symbols are the same as in Figure 7.

4.3 Sediment entrainment

The entrainment parameter X_i (Equation 11) is calculated for each grain-size class i of the near-bed suspended sediment samples, and plotted against the measured concentrations, where $E_s = \bar{c}_{b,i}/F_i$ (Figure 11a). The Yellow River data generally agree with the Wright and Parker (2004b) prediction (Equation 10): most measurements are within an order of magnitude of the predicted value. The largest and smallest grain-size classes show the largest deviation from the prediction (Figure 11b). In particular, $E_{s,i}$ of the smallest grain-size class (25 μm) extends several orders of magnitude below prediction, and the second-smallest class (43 μm) $E_{s,i}$ exceeds the hypothetical limit of a fluid of 0.3 (Wright & Parker, 2004a, recall that $E_{s,i}$ is a distribution-normalized measured concentration and not the true measured concentration).

On visual inspection of Figure 11a, it appears that the entrainment rates for samples collected in 2016 (circles, minor stratification effects) exceed prediction, whereas the entrainment rate for samples collected in 2018 (triangles, significant stratification) fall below prediction. This observation is quantified by the inset boxplots in Figure 11b. The median α_f is 0.60 when the measured concentration exceeds the predicted value by a factor of two (meas./pred.$>$2), whereas the median α_f is 0.36 when the measurement was less than half of the prediction (meas./pred.$<$0.5). These sample groups are statistically different, as determined by a Wilcoxon rank sum test ($p = 5.4 \times 10^{-5}$).

5 Discussion

5.1 Density stratification and sediment diffusivity

Direct measures of sediment-induced density stratification, both in laboratory and field settings, are limited. The normalized mean signed deviation and α_f statistics (Figures 7–8) confirm the presence of density stratification in the Yellow River, particularly at high sediment concentration. Furthermore, the grain-size specific calculations of the mean signed deviation and $\alpha_{f,i}$ show that sediment grain size is not uniformly stratified.

However, the patterns of density stratification documented herein (as α_f and $\alpha_{f,i}$) are confounded by sediment diffusivity, which also varies according to grain size and concentration. It is difficult to isolate these effects in natural flows, because sediment concentration and density stratification evolve non-linearly with increasing shear stress (Winterwerp, 2006). However, experimental studies have quantified sediment diffusivity coefficients in dilute suspension conditions, and concluded that β is predominately a function of grain size (van Rijn, 1984; Rose & Thorne, 2001; Graf & Cellino, 2002). Observations from the Yellow River confirm a grain-size dependence of sediment diffusivity (Figure 10b), as well as a dependence on concentration. A decrease in β with increasing concentration is consistent with observations of grain-grain collisions in the flow (Nezu & Azuma, 2004). Grain-size classes ≥ 122 μm consistently have positive fractional error values, and finer grain-size classes typically have negative fractional error values, as characterized by sediment diffusivity coefficient $\beta > 1$ for coarse sediments and $\beta \leq 1$ for fine sediment (e.g., van Rijn, 1984).

There is controversy surrounding the variability of β with distance above the bed. Rose and Thorne (2001) demonstrated β is independent of distance above the bed, yet Bennett et al. (1998) identified a pattern of variation of β with distance above the bed. Unfortunately, comparison of Rouse numbers (Figure 10a,b) and boundary condition effects of the buoyancy-stratified model ($\bar{c}_{MY}$, Figure 10c) preclude elucidating depth dependence in the Yellow River data. Buoyancy-stratified simulations using the Mellor and Yamada (1982) model and river concentration profiles, which allow a flexible boundary condition, may help to inform about sediment diffusivity behavior.

The variability in the behavior of sediment diffusivity has a net-zero effect on the adjustment coefficient (α_f) of the cumulative concentration profile, as seen by the agreement with the Wright and Parker (2004b) prediction (Figure 8a, Equation 8). However, grain-size profile adjustments scatter around the α_{WP04} prediction (Figure 8b), likely because this assumes $\beta = 1$. This suggests that sediment diffusivity is a second-order control on the shape of the concentration profile.

Density stratification is the primary control on the adjustment coefficient. There is a large change in α_f as concentration changes and suspended grain size is relatively fixed (Figures 5g–i, 8a). It might be expected that with increasing stress, a given grain size is more uniformly distributed. However, the trends in r_0 indicate that turbulence suppression due to density stratification overwhelms the concomitant increase in the u_*/w_s ratio; near-bed concentration increases significantly with increasing shear stress, but sediment is not distributed to the entire water column because turbulent mixing is inhibited. Thus, despite sediment diffusivity variability modulating grain-size specific concentration profiles, stratification is the primary control on profile shape and magnitude. Nevertheless, as a value of α greater than unity has no reasonable physical meaning (Wright & Parker, 2004a), α_f and $\alpha_{f,i}$ values greater than one are likely influenced by sediment diffusivity effects. Thus, when concentration is sufficiently low that stratification effects are minimal (i.e., the 2016 survey), the dominant control on profile shape is sediment diffusivity (Figures 8b and 10b).

5.2 Sediment entrainment

Entrainment relations seek to link flow and bed material properties to predict near-bed sediment concentration. Generally, the measured Yellow River sediment concentrations agree with the trend of the Wright and Parker (2004b) model (Equation 10) across grain-size classes, barring the largest and smallest grain-size classes (Figure 11a).

The increased variability of the largest grain-size class could be due to the distribution-normalizing procedure used to determine $E_{s,i}$. Alternatively, increasing sediment diffusivity of coarse grain sizes leads to higher than expected near-bed concentration, although, this would be inconsistent with the physical interpretation that increased sediment diffusivity requires particles be elevated from the bed by decaying turbulent eddies. Otherwise, larger variability in the instantaneous near-bed concentration may be due to the larger grain sizes concentrated there (Gitto et al., 2017).

The sediment entrainment rate of the finest grain-size class is approximately two orders of magnitude lower than predicted (Figure 11a). This is not a consequence of the treatment of washload sediment (< 15 μm), because F_i in the distribution-normalizing procedure to determine $E_{s,i}$ is the fraction of the washload-free suspended sediment samples. Instead, the lower than predicted entrainment is interpreted to result from sediment supply limitation in this grain-size class—consistent with the an expectation for sediment found in limited quantity on the bed. However, the sediment concentration in this class is positively correlated with λX_i, implying that sediment is indeed sourced from the bed. The implications of these observations are discussed in further detail below.

Variability in entrainment is correlated with density stratification (Figure 11b). Specifically, the samples collected in a flow with weaker density stratification show higher entrainment rates than predicted, whereas stratified flows reduce entrainment rates. This supports the notion that suppressed turbulence due to density stratification lowers entrainment (Vanoni, 1941).

5.3 Grain-size specific effects of stratification, and defining washload

There are varying definitions of washload (Woo et al., 1986), such as a combination of criteria including: 1) proportionally small quantities on the channel bed, 2) supply limitation, 3) a Rouse number suggesting uniform concentration (Hill et al., 2017), 4) finer than a defined grain size threshold (Partheniades, 1977), or 5) lack of contribution to change in channel-bed slope (Paola et al., 1999). In the Yellow River, fine sediment displays unexpected and interesting behavior that deviates from coarser grain-size classes (e.g., Figures 8b, 9b, and 11a). Specifically, the entrainment observations provide contradictory evidence for supply- and transport-limited sediment transport (Figure 11a), and the recovery coefficient (r_0) indicates that the finest grain-size class is non-uniformly distributed and stratified, which questions the appropriate definition of washload for this system. A supply limited finest grain-size class implies that the washload threshold used in this study (15 μm) is too fine, whereas non-uniform vertical distribution and stratification of the finest grain-size class suggests that the washload threshold may be too coarse.

The 5^{th} percentile of the channel bed grain-size distribution has been recognized to demarcate the threshold to washload (e.g., Woo et al., 1986). Based on this criterion, the Yellow River washload threshold would be 40–50 μm (Figure 5g–i). However, the upper-extent of supply limitation observed in entrainment measurements is between 25 μm and 43 μm (Figure 11a). The finest grain-size class has extremely small Rouse numbers (Figure 8b), yet this sediment contributes to the turbulent kinetic energy budget, and is not uniformly distributed in the flow (Figure 9b). Taken together, the observations are most consistent with a washload definition that incorporates a dimensionless shear velocity (e.g., a Rouse number, Equation 5; Hill et al., 2017). These observations underscore the importance of establishing a washload cutoff based on the research question of interest: it is necessary to consider even the finest

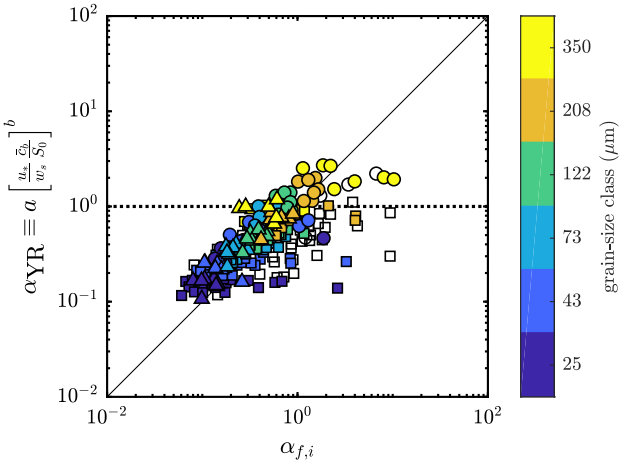

Figure 12: Correlation between grain-size specific $\alpha_{f,i}$ and predicted concentration profile adjustment from Equation 15.

sediment to study the turbulent energy budget for a flow, yet, a definition that considers material comprising the bed is appropriate for morphodynamic modeling, as this considers only material that affects the transport capacity of the flow (Paola et al., 1999; Li et al., 2015; Dong et al., 2019). This highlights the need to reexamine the behavior of fine sediment in open channel flows.

5.4 Adjustment to Rouse profiles

The α_{WP04} model (Equation 8) over-estimates the concentration in the upper half of the water column (Figure 5a–c, Supplementary Material) because the α_{WP04} model ignores grain-size specific variability in stratification effects (i.e., applies the same adjustment to each concentration profile). To address the grain-size dependent variability in stratification conditions, a modified prediction is proposed. The $\bar{c}_b/S_0$ ratio correlates strongly with bulk density stratification effects, and this ratio offers an independent variable in the α_{WP04} relation (Equation 8), but precludes grain-size specific stratification effects. The data from this study are recast in terms of a multivariate linear regression, whereby the eddy viscosity adjustment coefficient ($\alpha_{f,i}$) is dependent on the sand-river Richardson number (Equation 7, Figure 12). The regression equation obtained is:

$$\alpha_{\mathrm{YR,i}} = a\left[\frac{u_*}{w_{s,i}}\frac{\bar{c}_b}{S_0}\right]^b, \tag{15}$$

where $a = 7.3$ and $b = -0.39$ ($\mathrm{r}^2 = 0.51$). The finest and coarsest grain-size classes are omitted from the regression, because they often have extreme values. Nevertheless, these data plot along the same trend as the center-distribution grain-size classes (Figure 12). The relation predicts the *total* adjustment to the concentration profile, and so includes density stratification and sediment diffusivity. The formulation depicts the distribution of turbulent kinetic energy specifically in the case of the Yellow River, and should therefore be applied cautiously to other rivers.

The bulk stratification coefficient remains a useful metric in other rivers, and a relation incorporating grain size, concentration, and slope is generated for a constant slope, by defining auxiliary variables m and n:

$$\alpha_{S_0} = 1 - \left[m\,(\bar{c}_b \mathrm{Re}_{\mathrm{p},50}^{-0.6})^n\right], \tag{16}$$

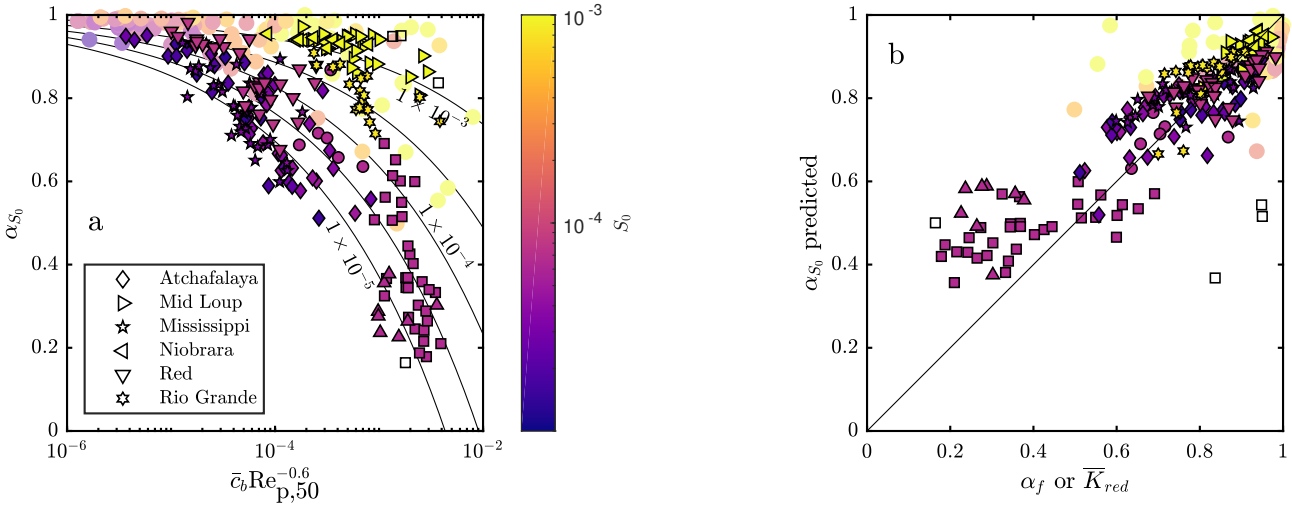

Figure 13: a) Depth-averaged reduction in eddy viscosity as a function of near-bed concentration and particle Reynolds number. Rivers separate along contours of channel-bed slope. b) Correlation between measured and predicted α by Equation 16.

where $m = -2.2(\log_{10} S_0) - 5.2$ and $n = 0.017(\log_{10} S_0) + 0.40$, and $\mathrm{Re}_{\mathrm{p50}}$ is the particle Reynolds number of the median grain size of bed material ($\mathrm{r}^2 = 0.82$, Figure 13). For the purposes of this regression, the data from Wright and Parker (2004a, 2004b) are treated as field-validated data. A larger dataset of concentration profiles from global rivers is likely to improve predictions.

Simulations were performed with the buoyancy-stratified model, using a global dataset of river properties as the boundary condition (Li et al., 2015); the sediment mixture is assumed to be single-size and entrainment follows Equation 10 (Wright & Parker, 2004b). This set of simulations follows similar trends to the separation identified by α_{S_0} (Equation 16). Additional $\bar{c}_{MY}$ simulations are randomly sampled from the parameter space of the dataset of global rivers from Li et al. (2015), and the depth-averaged eddy viscosity is never reduced below $\overline{K}_{red} = 0.25$ (Supplementary Material). This is consistent with the Yellow River measurements, where $\alpha_f \approx 0.2$ was the minimum value. This may represent a physical limit to the reduction of the eddy viscosity profile, and could inform turbulent kinetic energy budgets of other river systems. Alternatively, this may be a numerical artifact relating to extinguished turbulence (e.g., Wright & Parker, 2004a). An area of focus for future work is to systematically explore this lower limit, by manipulating suspension properties like grain size, slope, and concentration.

5.5 Predicting sediment transport

The suspended sediment flux in a river is impacted by density stratification (Figure 14; Vanoni, 1941, 1946; Wright & Parker, 2004a), whereby sediment flux is less than predicted using log-law velocity and Rouse concentration profiles ($\alpha = 1$, Equations 3–5). Predicting the depth-averaged density stratification coefficient α and applying the adjusted log-law velocity and Rouse concentration profiles improves sediment flux calculations. However, more velocity and concentration profile data are needed for a wide range of rivers to provide further validation.

Density stratification reduces sediment concentration in the upper portion of the water column, and when combined with sediment diffusivity, modulates the grain size distribution. This is important because engineered sediment

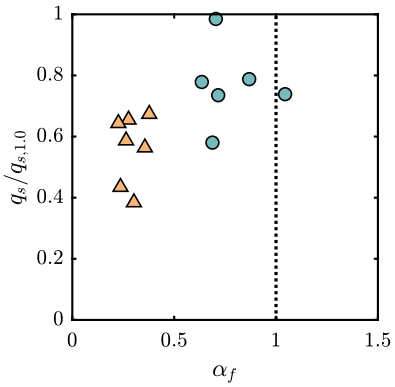

Figure 14: Ratio of width-averaged sediment transport (Equation 1) under density-stratified flow to predicted transport assuming a dilute suspension ($\alpha = 1$ in Equations 3–4).

diversions typically off-take the upper portion of flow (e.g., Nittrouer & Viparelli, 2014). Yet, to maximize coarse material flux, should draw water from the lower region of flow, where coarse material is focused. In the Yellow River, the grain-size distribution in the upper 20% of the flow is finer than predicted by the dilute-suspension model (validated by Wilcoxon signed rank test, Supplementary Material) and the overall sediment concentration is $18 \pm 10\%$ lower.

The buoyancy stratified model of Mellor and Yamada (1982) accurately predicts the cumulative grain-size concentration profiles across the full range of observed density stratification (Supplementary Material). The stratification conditions documented in this study are among the strongest observed in any natural open-channel flow, which means that the buoyancy-stratified model is likely accurate for other flow and sediment-mixture conditions. While the Mellor and Yamada (1982) model is analytically complex, software packages provide a simple method to predict suspension conditions (e.g., Yeh & Parker, 2013). These packages should be widely adopted when designing sediment diversion structures, because projects targeting large low-sloping rivers are prone to density stratification effects (Wright & Parker, 2004a, 2004b).

6 Conclusions

Density stratification is found in suspended sediment concentration profiles in the Yellow River. The density stratification effect is enhanced for fine sediment relative to coarse sediment, whereby the coarsest sediment is relatively unaffected. Measured concentration profiles are modulated by both density stratification and sediment diffusivity, however, density stratification exerts a primary control on the velocity and concentration profiles. However, at low sediment concentration, variation in the sediment diffusivity significantly impacts the vertical distribution of sediment grain size. The sediment diffusivity documented in the Yellow river is consistent with an momentum effect for coarser sediment ($\beta > 1$) and a lagging inertial effect impacts finer sediment. Sediment entrainment is correlated with density stratification, whereby entrainment is reduced by suppressed turbulence near the bed in stratified flow. Fine sediment suspended in the river appears to be supply limited and is only sparsely present on the channel bed, yet this material is not uniformly distributed in the vertical and changes concentration with increasing shear stress. This suggests that even very fine sediment extracts turbulent energy from the flow, and that the washload threshold grain-size in the Yellow River is fine ($< 25\ \mu$m).

Acknowledgments

A.J.M., J.A.N., H.M., B.N.C., M.P.L., and G.P. acknowledge support from the National Science Foundation (NSF) EAR-1427262 Coastal SEES grant. A.J.M. was supported by a NSF Graduate Research Fellowship under Grant No. 1842494. The data, and processing and analysis code, are made available online. Processed and raw datasets can be found at Zenodo `https://zenodo.org/record/3457639`, and the processing and plotting scripts can be found at `https://github.com/amoodie/paper_resources/Moodie_densitystratification`, on publication of the peer-reviewed manuscript.

References

Amoudry, L. (2005). Schmidt number and near-bed boundary condition effects on a two-phase dilute sediment transport model. *Journal of Geophysical Research*, *110*(C9). doi: 10.1029/2004JC002798

An, C., Moodie, A. J., Ma, H., Fu, X., Zhang, Y., Naito, K., & Parker, G. (2018). Morphodynamic model of lower Yellow River: flux or entrainment form for sediment mass conservation? *Earth Surface Dynamics*, *6*(4), 989–1010. doi: 10.5194/esurf-6-989-2018

Anderson, A. G. (1942). Distribution of suspended sediment in a natural stream. *Transactions, American Geophysical Union*, *23*(2), 678. doi: 10.1029/TR023i002p00678

Barton, J., & Lin, P. (1955). *A Study of the Sediment Transport in Alluvial Channels*. Colorado A and M College, Civil Engineering Department.

Bennett, S. J., Bridge, J. S., & Best, J. L. (1998, January). Fluid and sediment dynamics of upper stage plane beds. *Journal of Geophysical Research: Oceans*, *103*(C1), 1239–1274. doi: 10.1029/97JC02764

Cao, Z., Pender, G., & Carling, P. (2006, April). Shallow water hydrodynamic models for hyperconcentrated sediment-laden floods over erodible bed. *Advances in Water Resources*, *29*(4), 546–557. doi: 10.1016/j.advwatres.2005.06.011

Cellino, M., & Graf, W. H. (1999, May). Sediment-Laden Flow in Open-Channels under Noncapacity and Capacity Conditions. *Journal of Hydraulic Engineering*, *125*(5), 455–462. doi: 10.1061/(ASCE)0733-9429(1999)125:5(455)

Chan-Braun, C., Garcia-Villalba, M., & Uhlmann, M. (2010, June). Numerical Simulation of fully resolved particles in rough-wall turbulent open channel flow. In *ICMF 2010*. Tampa, FL.

Colby, B. R. (1964). *Discharge of Sands and Mean-Velocity Relationships in Sand-Bed Streams* (Tech. Rep. No. GEOLOGICAL SURVEY PROFESSIONAL PAPER 462-A).

Colby, B. R., & Hembree, C. H. (1955). *Computations of Total Sediment Discharge Niobrara River Near Cody, Nebraska* (Tech. Rep. No. GEOLOGICAL SURVEY WATER-SUPPLY PAPER 1357).

Coleman, N. L. (1970, June). Flume Studies of the Sediment Transfer Coefficient. *Water Resources Research*, *6*(3), 801–809. doi: 10.1029/WR006i003p00801

Coleman, N. L. (1981, July). VELOCITY PROFILES WITH SUSPENDED SEDIMENT. *Journal of Hydraulic Research*, *19*(3), 211–229. doi: 10.1080/00221688109499516

Coleman, N. L. (1986, September). Effects of Suspended Sediment on the Open-Channel Velocity Distribution. *Water Resources Research*, *22*(10), 1377–1384. doi: 10.1029/WR022i010p01377

Cornell, K. M. (2007). *Suspended Sediment Erosion in Laboratory Flume Experiments* (MS Thesis). Massachusetts Institute of Technology.

Dietrich, W. E. (1982, December). Settling velocity of natural particles. *Water Resources Research*, *18*(6), 1615–1626. doi: 10.1029/WR018i006p01615

Dong, T. Y., Nittrouer, J. A., Czapiga, M. J., Ma, H., McElroy, B., Il'icheva, E., ... Parker, G. (2019, January). Roles of Bank Material in Setting Bankfull Hydraulic Geometry as Informed by the Selenga River Delta, Russia. *Water Resources Research*, *55*(1), 827–846. doi: 10.1029/2017WR021985

Doshi, M. R., & Gill, W. N. (1970, September). A note on the mixing length theory of turbulent flow. *AIChE Journal*, *16*(5), 885–888. doi: 10.1002/aic.690160532

Duan, J. G., & Nanda, S. (2006, August). Two-dimensional depth-averaged model simulation of suspended sediment concentration distribution in a groyne field. *Journal of Hydrology*, *327*(3-4), 426–437. doi: 10.1016/j.jhydrol .2005.11.055

Einstein, H., & Chien, N. (1955). *Effects of Heavy Sediment Concentration Near the Bed on Velocity and Sediment Distribution*. U.S. Army Engineer Division, Missouri River.

Galperin, B., Kantha, L. H., Hassid, S., & Rosati, A. (1988, January). A Quasi-equilibrium Turbulent Energy Model for Geophysical Flows. *Journal of the Atmospheric Sciences*, *45*(1), 55–62. Retrieved 2019-08-20, from `http://journals.ametsoc.org/doi/abs/10.1175/1520-0469%281988%29045%3C0055%3AAQETEM%3E2.0.CO%3B2` doi: 10.1175/1520-0469(1988)045⟨0055:AQETEM⟩2.0.CO;2

Ganti, V., Chu, Z., Lamb, M. P., Nittrouer, J. A., & Parker, G. (2014, November). Testing morphodynamic controls on the location and frequency of river avulsions on fans versus deltas: Huanghe (Yellow River), China: Avulsion drivers on fans versus deltas. *Geophysical Research Letters*, *41*(22), 7882–7890. doi: 10.1002/2014GL061918

García, M., & Parker, G. (1991, April). Entrainment of Bed Sediment into Suspension. *Journal of Hydraulic Engineering*, *117*(4), 414–435. doi: 10.1061/(ASCE)0733-9429(1991)117:4(414)

García, M., & Parker, G. (1993). Experiments on the entrainment of sediment into suspension by a dense bottom current. *Journal of Geophysical Research*, *98*(C3), 4793. doi: 10.1029/92JC02404

García, M. H. (2008). Ch 2: Sediment Transport and Morphodynamics. In *Sedimentation engineering processes, measurements, modeling, and practice* (pp. 21–163). Reston, VA.: American Society of Civil Engineers.

Gelfenbaum, G., & Smith, J. D. (1986). Experimental Evaluation of a Generalized Suspended-Sediment Transport Theory. In *Shelf Sands and Sandstones* (pp. 133–144).

Ghoshal, K., & Mazumder, B. S. (2005, November). Sediment-induced stratification in turbulent open-channel flow. *Environmetrics*, *16*(7), 673–686. doi: 10.1002/env.729

Ghoshal, K., & Pal, D. (2014, June). Grain-size distribution in suspension over a sand-gravel bed in open channel flow. *International Journal of Sediment Research*, *29*(2), 184–194. doi: 10.1016/S1001-6279(14)60035-4

Gitto, A. B., Venditti, J. G., Kostaschuk, R., & Church, M. (2017, April). Representative point-integrated suspended sediment sampling in rivers: REPRESENTATIVE SEDIMENT SAMPLING. *Water Resources Research*, *53*(4), 2956–2971. doi: 10.1002/2016WR019187

Graf, W. H., & Cellino, M. (2002). Suspension flows in open channels; experimental study. *Journal of Hydraulic Research*, *40*(4), 435-447. doi: 10.1080/00221680209499886

Greimann, B. P., Muste, M., & Holly, F. M. (1999, July). Two-phase formulation of suspended sediment transport. *Journal of Hydraulic Research*, *37*(4), 479–500. doi: 10.1080/00221686.1999.9628264

Hill, K. M., Gaffney, J., Baumgardner, S., Wilcock, P., & Paola, C. (2017, January). Experimental study of the effect of grain sizes in a bimodal mixture on bed slope, bed texture, and the transition to washload: BIMODAL XPORT: SLOPE, TEXTURE, & WASHLOAD. *Water Resources Research*, *53*(1), 923–941. doi: 10.1002/2016WR019172

Hsu, T.-J., Jenkins, J. T., & Liu, P. L.-F. (2004, August). On two-phase sediment transport: sheet flow of massive particles. *Proceedings of the Royal Society A: Mathematical, Physical and Engineering Sciences*, *460*(2048), 2223–2250. doi: 10.1098/rspa.2003.1273

Jobson, H. (1970). Vertical Transfer in Open Channel Flow. *Journal of the Hydraulics Division*, *96*(3), 703–724.

Lamb, M. P., & Parsons, J. D. (2005, May). High-Density Suspensions Formed Under Waves. *Journal of Sedimentary Research*, *75*(3), 386–397. doi: 10.2110/jsr.2005.030

Lees, B. J. (1981, September). Relationship between eddy viscosity of seawater and eddy diffusivity of suspended particles. *Geo-Marine Letters*, *1*(3-4), 249–254. doi: 10.1007/BF02462442

Leopold, L. B., Wolman, M. G., & Miller, J. P. (1995). *Fluvial processes in geomorphology* (Dover ed ed.). New York: Dover Publications.

Li, C., Czapiga, M. J., Eke, E. C., Viparelli, E., & Parker, G. (2015, January). Variable Shields number model for river bankfull geometry: bankfull shear velocity is viscosity-dependent but grain size-independent. *Journal of Hydraulic Research*, *53*(1), 36–48. doi: 10.1080/00221686.2014.939113

Lyn, D. A. (1986). *Turbulence and Turbulent Transport in Sediment-laden Open-channel Flows* (PhD Thesis). California Institute of Technology, Pasadena, California.

Ma, H., Nittrouer, J. A., Naito, K., Fu, X., Zhang, Y., Moodie, A. J., ... Parker, G. (2017). The exceptional sediment load of fine-grain dispersal systems: Example of the yellow river, china. , *3*, 7. doi: 10.1126/sciadv.1603114

Ma, H., Nittrouer, J. A., Wu, B., Lamb, M. P., Zhang, Y., Mohrig, D., ... Parker, G. (2020). Universal relation with regime transition for sediment transport in fine-grained rivers. *Proceedings of the National Academy of Sciences*. doi: 10.1073/pnas.1911225116

McLean, S. R. (1991, November). Depth-Integrated Suspended-Load Calculations. *Journal of Hydraulic Engineering*, *117*(11), 1440–1458. doi: 10.1061/(ASCE)0733-9429(1991)117:11(1440)

McLean, S. R. (1992). On the calculation of suspended load for noncohesive sediments. *Journal of Geophysical Research*, *97*(C4), 5759. doi: 10.1029/91JC02933

McLean, S. R., Nelson, J. M., & Wolfe, S. R. (1994). Turbulence structure over two-dimensional bed forms: Implications for sediment transport. *Journal of Geophysical Research*, *99*(C6), 12729. doi: 10.1029/94JC00571

Mellor, G. L., & Yamada, T. (1982). Development of a turbulence closure model for geophysical fluid problems. *Reviews of Geophysics*, *20*(4), 851–875. doi: 10.1029/RG020i004p00851

Milliman, J. D., & Meade, R. H. (1983, January). World-Wide Delivery of River Sediment to the Oceans. *The Journal of Geology*, *91*(1), 1–21. doi: 10.2307/30060512

Moodie, A. J. (2019). *Yellow River Kenli Lijin Station Survey* [dataset]. doi: 10.5281/zenodo.3457639

Moodie, A. J., Nittrouer, J. A., Ma, H., Carlson, B. N., Chadwick, A. J., Lamb, M. P., & Parker, G. (2019). Modeling deltaic lobe-building and channel avulsions for the Yellow River delta, China. *Journal of Geophysical Research: Earth Surface*. doi: 10.1029/2019JF005220

Murray, S. P. (1970, March). Settling velocities and vertical diffusion of particles in turbulent water. *Journal of Geophysical Research*, *75*(9), 1647–1654. doi: 10.1029/JC075i009p01647

Nezu, I., & Azuma, R. (2004, October). Turbulence Characteristics and Interaction between Particles and Fluid in Particle-Laden Open Channel Flows. *Journal of Hydraulic Engineering*, *130*(10), 988–1001. doi: 10.1061/(ASCE)0733-9429(2004)130:10(988)

Nezu, I., & Rodi, W. (1986, May). Open-channel Flow Measurements with a Laser Doppler Anemometer. *Journal of Hydraulic Engineering*, *112*(5), 335–355. doi: 10.1061/(ASCE)0733-9429(1986)112:5(335)

Nikuradse, J. (1926). *Laws of Flow in Rough Pipes, translation of Stromungsgesetze in rauhen Rohren* (Tech. Rep. No. NACA-TM-1292). (Report Date: Nov 01, 1950)

Nittrouer, J. A., Allison, M. A., & Campanella, R. (2008, July). Bedform transport rates for the lowermost Mississippi River. *Journal of Geophysical Research*, *113*(F3). doi: 10.1029/2007JF000795

Nittrouer, J. A., Mohrig, D., & Allison, M. (2011, December). Punctuated sand transport in the lowermost Mississippi River. *Journal of Geophysical Research*, *116*(F4). doi: 10.1029/2011JF002026

Nittrouer, J. A., Shaw, J., Lamb, M. P., & Mohrig, D. (2012, March). Spatial and temporal trends for water-flow velocity and bed-material sediment transport in the lower Mississippi River. *Geological Society of America Bulletin*, *124*(3-4), 400–414. doi: 10.1130/B30497.1

Nittrouer, J. A., & Viparelli, E. (2014, April). Sand as a stable and sustainable resource for nourishing the Mississippi River delta. *Nature Geoscience*, *7*(5), 350–354. doi: 10.1038/ngeo2142

Nordin, C. F., & Dempster, G. R. (1963). *Vertical Distribution of Velocity and Suspended Sediment Middle Rio Grande, New Mexico* (Tech. Rep. No. GEOLOGICAL SURVEY PROFESSIONAL PAPER 462-B).

Paola, C., Parker, G., Mohrig, D. C., & Whipple, K. X. (1999). The influence of transport fluctuations on spatially averaged topography on a sandy, braided fluvial fan. In *Numerical Experiments in Stratigraphy: Recent Advances in Stratigraphic and Sedimentologic Computer Simulations* (pp. 211–218). Society for Sedimentary Geology.

Parker, G., & Coleman, N. L. (1986, May). Simple Model of Sediment-Laden Flows. *Journal of Hydraulic Engineering*, *112*(5), 356–375. doi: 10.1061/(ASCE)0733-9429(1986)112:5(356)

Partheniades, E. (1977). Unified View of Wash Load and Bed Material Load. *Journal of the Hydraulics Division*, *103*(9), 1037–1057.

Ren, M.-e., & Walker, H. J. (1998, October). Environmental consequences of human activity on the Yellow River and its delta, China. *Physical Geography*, *19*(5), 421–432.

Rose, C. P., & Thorne, P. D. (2001, October). Measurements of suspended sediment transport parameters in a tidal estuary. *Continental Shelf Research*, *21*(15), 1551–1575. doi: 10.1016/S0278-4343(00)00087-X

Rouse, H. (1937). Modern Conceptions of the Mechanics or Fluid Turbulence. *Transactions of the American Society of Civil Engineers*, *102*(1), 463–505.

Rouse, Hunter. (1939). *An Analysis of Sediment Transportation in the Light of Fluid Turbulence.* United States Department of Agriculture, Washington, DC. Retrieved from `https://resolver.caltech.edu/CaltechAUTHORS:20140529-132455484`

Saito, Y., Wei, H., Zhou, Y., Nishimura, A., Sato, Y., & Yokota, S. (2000, August). Delta progradation and chenier formation in the Huanghe (Yellow River) delta, China. *Journal of Asian Earth Sciences*, *18*(4), 489–497. doi: 10.1016/S1367-9120(99)00080-2

Saito, Y., Yang, Z., & Hori, K. (2001, November). The Huanghe (Yellow River) and Changjiang (Yangtze River) deltas: a review on their characteristics, evolution and sediment discharge during the Holocene. *Geomorphology*, *41*(2-3), 219–231. doi: 10.1016/S0169-555X(01)00118-0

Smith, J. D. (1977). *Modeling of sediment transport on continental shelves*. University of Washington, Dept. of Oceanography.

Smith, J. D., & McLean, S. (1977a). Boundary Layer Adjustments to Bottom Topography and Suspended Sediment. In *Elsevier Oceanography Series* (Vol. 19, pp. 123–151). Elsevier. (DOI: 10.1016/S0422-9894(08)70839-0)

Smith, J. D., & McLean, S. R. (1977b, April). Spatially averaged flow over a wavy surface. *Journal of Geophysical Research*, *82*(12), 1735–1746. doi: 10.1029/JC082i012p01735

Turner, J. S. (1979). *Buoyancy effects in fluids* (1. paperback ed ed.). Cambridge: Cambridge Univ. Press. (OCLC: 637416666)

van Gelder, A., van den Berg, J. H., Cheng, G., & Xue, C. (1994, May). Overbank and channelfill deposits of the modern Yellow River delta. *Sedimentary Geology*, *90*(3–4), 293–305. doi: 10.1016/0037-0738(94)90044-2

van Ingen, C. (1981). *Observations in a sediment-laden flow by use of laser-doppler velocimetry* (Tech. Rep. No. KH-R-42). Pasadena, California: W. M. Keck Laboratory of Hydraulics and Water Resources. (doi: 10.7907/Z9QF8QTP)

Vanoni, V. A. (1941). Some experiment on the transporation of suspended load. *Transactions, American Geophysical Union*, *22*(3), 608. doi: 10.1029/TR022i003p00608

Vanoni, V. A. (1946). Transportation of sediment by water. *Transactions of the AGU*, *3*, 67–133.

Vanoni, V. A. (1980). *Sediment studies in the Brazilian Amazon River basin* (Tech. Rep. Nos. United Nations Development Program, Report KH-P-168). W. M. Keck Laboratoty of Hydraulics and Water Resources: California Institute of Technology, Pasadena, California.

Vanoni, V. A. (Ed.). (2006). *Sedimentation Engineering* (Classic ed.). Reston, VA: American Society of Civil Engineers.

van Rijn, L. C. (1984, November). Sediment Transport, Part II: Suspended Load Transport. *Journal of Hydraulic Engineering*, *110*(11), 1613–1641. doi: 10.1061/(ASCE)0733-9429(1984)110:11(1613)

Villaret, C., & Trowbridge, J. H. (1991). Effects of stratification by suspended sediments on turbulent shear flows. *Journal of Geophysical Research*, *96*(C6), 10659. doi: 10.1029/91JC01025

Wang, Z.-Y., & Liang, Z.-Y. (2000, July). Dynamic characteristics of the Yellow River mouth. *Earth Surface Processes and Landforms*, *25*(7), 765–782. doi: 10.1002/1096-9837(200007)25:7$\langle$$765::AID-ESP98$\rangle$$3.0.CO;2-K

Whitehouse, R. (1995, November). Observations of the boundary layer characteristics and the suspension of sand at a tidal site. *Continental Shelf Research*, *15*(13), 1549–1567. doi: 10.1016/0278-4343(95)00038-3

Winterwerp, J. C. (2006). Stratification effects by fine suspended sediment at low, medium, and very high concentrations. *Journal of Geophysical Research*, *111*(C5). doi: 10.1029/2005JC003019

Woo, H. S., Julien, P. Y., & Richardson, E. V. (1986). Washload and fine sediment load. *Journal of Hydraulic Engineering*, *112*(6), 541–545.

Wright, S., & Parker, G. (2004a, August). Density Stratification Effects in Sand-Bed Rivers. *Journal of Hydraulic Engineering*, *130*(8), 783–795. doi: 10.1061/(ASCE)0733-9429(2004)130:8(783)

Wright, S., & Parker, G. (2004b, August). Flow Resistance and Suspended Load in Sand-Bed Rivers: Simplified Stratification Model. *Journal of Hydraulic Engineering*, *130*(8), 796–805. doi: 10.1061/(ASCE)0733-9429(2004)130:8(796)

Yeh, T.-h., & Parker, G. (2013, April). Software for evaluating sediment-induced stratification in open-channel flows. *Computers & Geosciences*, *53*, 94–104. Retrieved 2019-09-16, from `https://linkinghub.elsevier.com/retrieve/pii/S0098300411004286` doi: 10.1016/j.cageo.2011.12.004

Yu, L. (2002, February). The Huanghe (Yellow) River: a review of its development, characteristics, and future management issues. *Continental Shelf Research*, *22*(3), 389–403. doi: 10.1016/S0278-4343(01)00088-7

Zhang, S., & Duan, J. G. (2011, July). 1d finite volume model of unsteady flow over mobile bed. *Journal of Hydrology*, *405*(1-2), 57–68. doi: 10.1016/j.jhydrol.2011.05.010

Zhang, S., Duan, J. G., & Strelkoff, T. S. (2013, January). Grain-Scale Nonequilibrium Sediment-Transport Model for Unsteady Flow. *Journal of Hydraulic Engineering*, *139*(1), 22–36. doi: 10.1061/(ASCE)HY.1943-7900.0000645